THE ASTROPHYSICAL JOURNAL, 435:79–92, 1994 November 1

INTERACTING BINARY GALAXIES. VII. KINEMATIC DATA FOR 12 DISTURBED ELLIPTICALS

KIRK D. BORNE[1]
Space Telescope Science Institute,[2] 3700 San Martin Drive, Homewood Campus, Baltimore, MD 21218
MARC BALCELLS
Kapteyn Astronomical Institute, Postbus 800, 9700 AV Groningen, The Netherlands
JOHN G. HOESSEL[1]
Washburn Observatory, University of Wisconsin, 475 N. Charter Street, Madison, WI 53706
AND
MATTHEW MCMASTER
Space Telescope Science Institute,[2] 3700 San Martin Drive, Homewood Campus, Baltimore, MD 21218
Received 1994 January 26; accepted 1994 May 6

ABSTRACT

We have analyzed long-slit spectroscopic data for a sample of 12 tidally disturbed elliptical galaxies. The spectra were obtained with the KPNO 4 m RC spectrograph. Rotation curves and velocity dispersion profiles have been measured at a variety of position angles in these galaxies and have been used to analyze the dynamical response and internal kinematics of stellar systems involved in strong gravitational encounters. We have confirmed with these data our previous observation that such galaxies often reveal U-shaped "rotation" profiles, indicative of a strong resonant tidal effect among those stars that are moving prograde with respect to the galactic encounter. Additional kinematic peculiarities, including U-shaped and W-shaped velocity dispersion profiles, are also revealed in these data. The observed morphologies of the tidal features seen in some of the sample galaxies are consistent with the idea that elliptical galaxies often contain an embedded disk component. Our velocity profiles along new position angles confirm the validity of tidal interaction models that we previously derived for specific pairs in our sample using only a single slit position angle per galaxy. Additional insight into possible refinements of those collision models has also resulted from this study.

Subject headings: galaxies: interactions — galaxies: kinematics and dynamics

1. INTRODUCTION

Our information on the dynamics of elliptical galaxies has grown more wondrous and diverse over the past two decades as more advanced detectors have been applied to the problem. From the realization that the flattening of bright ellipticals is not rotationally supported (Bertola & Capaccioli 1975; Illingworth 1977) to the discovery of cores with rotation misaligned with respect to that of the main body of the galaxy (Franx & Illingworth 1988; Jedrzejewsky & Schechter 1988; Bender 1988), we now believe that these galaxies are not nearly so dull or so well understood as was once thought. Among the more unusual properties are the peculiar U-shaped rotation profiles that we discovered using the High Gain Video Spectrometer (HGVS) at the KPNO 4 m telescope. These were found in ~50% of the ellipticals that were selected on the basis of their strong interaction with a nearby companion galaxy (Borne & Hoessel 1985, 1988; Borne 1990a). In agreement with our findings, Madejsky, Bender, & Möllenhoff (1991) found U-shaped rotation profiles along some position angles in each member of the NGC 4782/4783 interacting pair (with an inverted U in NGC 4782, the higher-velocity component). NGC 205, the tidally disturbed companion to M31, shows clear evidence for a U-shaped dispersion profile (Bender, Paquet, & Nieto 1991), and the authors speculate that it may also have a very low-amplitude U-shaped rotation profile. We have shown that these unusual nonsteady rotation velocity fields are the result of momentum and energy transfer from the binary galaxy orbit into individual stellar orbits, which is leading to the orbital decay and impending merger of the interacting galaxy pair (Borne 1990b). The detection of peculiar motions of this type thus provides solid evidence for the action of tidal friction in colliding galaxies. Very little hard dynamical evidence of this kind has been presented despite the plethora of gravitational interaction simulations in the literature.

In Figure 1 we show a composite of the rotation profiles for four interacting ellipticals obtained from our HGVS data (reproduced from Borne 1990a). One can see that the evidence from any individual galaxy is weak, while the combined data show quite clearly the consistent behavior of the U-shaped profiles.

Our previous studies also indicated the presence of U-shaped dispersion profiles in interacting ellipticals. Recent data from Madejsky (1991) for NGC 750/751, from Madejsky et al. (1991) for NGC 4782/4783, and from Bender et al. (1991) for NGC 205 are in agreement with this finding.

For a more complete understanding of the "U-shape" phenomenon, both the quality and the quantity of these velocity curves must be improved. We have improved the quality of the spectroscopic observations by using the newer CCD detectors at KPNO, resulting in higher S/N measurements in the centers of the galaxies and in velocity measurements out to larger

[1] Visiting Astronomer, Kitt Peak National Observatory, National Optical Astronomy Observatories, operated by the Association of Universities for Research in Astronomy, Inc., under contract with the National Science Foundation.

[2] Operated by the Association of Universities for Research in Astronomy, Inc., for the National Aeronautics and Space Administration.

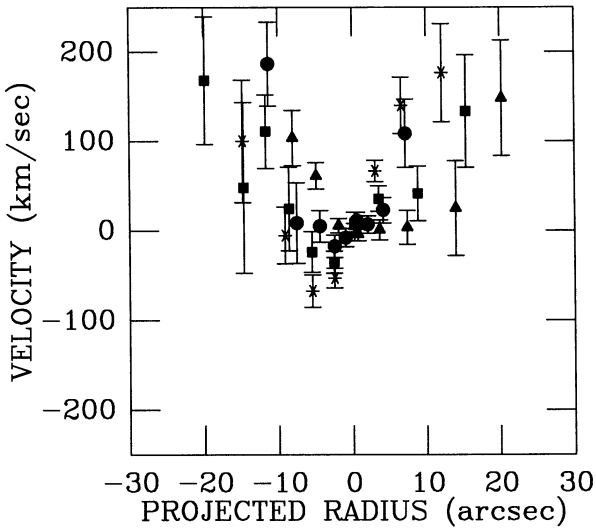

FIG. 1.—U-shaped rotation profiles for four tidally disturbed ellipticals. Data obtained with KPNO 4 m HGVS. The zero values of projected radius and velocity correspond to the central brightness peak in the given galaxy. Velocities are plotted for NGC 2673 (*circles*), NGC 7236 (*squares*), NGC 1588 (*triangles*), and IC 413 (*asterisks*).

radii, at fainter surface brightness. We have increased the quantity of data both through the study of a wider sample of interacting ellipticals and by measuring velocities at additional position angles in those galaxies that already showed evidence for a U-shaped rotation profile at the one previously studied position angle.

We previously analyzed our best HGVS velocity data along with multicolor CCD images in a series of papers where we presented collision simulations for four distorted pairs (Borne 1990a, and references therein). In each case, a dynamical configuration was found that completely matched our measured velocities and the observed optical morphology of the system. Forced to reproduce all of the available observations, the derived collision model was well constrained by the data and provided us with the complete mass, orbital, and spatial solution for each galaxy pair. For four pairs we found a small range of mass-to-light ratios, $M/L_B = 10\text{–}16h_{100}(\pm 2h_{100})M_\odot/L_\odot$ and a wide range of encounter trajectories (from bound to strongly unbound orbits). By increasing the available input data for this task, it is now possible to extend our knowledge about these fundamental galaxy parameters and to gain more observational insight into the dynamical friction process.

In addition to helping find new binary collision solutions, our long-slit spectroscopic measurements can be used to elucidate the internal dynamics of elliptical galaxies involved in collisions and to test the predictions of our published collision models. The observed disturbances in the velocity field of a tidally distorted galaxy can be used to probe the gravitational field of the interacting pair, leading to a better understanding of the internal structure, kinematics, and mass distribution of ellipticals in general. High-quality multiposition angle data are required for this. We have several good candidates among our interacting elliptical sample for such a detailed velocity mapping. Among these are NGC 1587 (with very fast rotation; Borne & Hoessel 1988 [Paper III]; Borne 1988b [Paper IV]), NGC 1588 (with U-shaped rotation; Paper III), NGC's 4782/4783 (tidally shocked and truncated; Borne, Balcells, & Hoessel 1988 [Paper V]), and NGC 2673 (with tidal plumes, tidal heating, U-shaped rotation, plus fast pre- and postcollision rotation predicted by our model; Balcells, Borne, & Hoessel 1989 [Paper VI]). Measurements of the velocity fields in such systems can be used both to validate more fully the models presented in the papers referenced here and to probe the internal kinematics of perturbed gravitating systems in general.

We report here on observations of Arp 171 (NGC 5718/IC 1042; from the catalog of Arp 1966), K46 (NGC 750/751), K99 (NGC 1587/1588), K175 (NGC 2672/2673), K194 (NGC 2802/2803), and K564 (NGC 7236/7237); the last five systems were selected from the catalog of isolated pairs published by Karachentsev (1972). The spectroscopic observations are supplemented by multicolor CCD imaging. HGVS observations for three of these objects have already been discussed by us in earlier papers (i.e., K99, K175, and K564). The other pairs were selected because their morphologies led us to believe that they are of similar character to those already analyzed. As pointed out by Borne (1988a [Paper II]), the success of the detailed and unique matching of collision simulations to observational data depends critically upon the availability of line-of-sight velocity and velocity dispersion measurements at several positions in the galaxies. Our expanded data set serves that purpose.

We describe the observations and their analysis in § 2. The results of that analysis are described and discussed in § 3. Comparisons between our new observations with predictions of our previously published collision models are presented in § 4. In § 5 we discuss the evidence for U-shaped rotation curves in the light of the new data. Finally, we offer in § 6 a general discussion of what we have learned about galaxy collisions and dynamical friction through this work.

2. OBSERVATIONS

2.1. *Velocity Measurements*

We used the RC spectrograph on the KPNO 4 m telescope to obtain long-slit spectra of several pairs of interacting elliptical galaxies. Observations were made on two observing runs with two different detectors. In 1990 February we used the bare TI CCD, and in 1990 November we used the Tektronix 1024 CCD.

We list in Table 1 the instrument parameters for our two observing runs. In each case the output image included 32 columns for bias overscan. For the TI CCD, we actually double-binned the pixels in the spatial direction prior to readout. For each observing run, our chosen slit width of 2″ corresponded to a physical slit width of 300 μm.

TABLE 1

INSTRUMENT PARAMETERS

Date	CCD	Format	Read Noise	Slit	Spatial Scale	FWHM (2″ slit)	Grating	λ Scale (Å pixel^{-1})	λ Range (Å)
1990 Feb	TI	432 × 800	~10 e^-	5.7	0.″86/pixel	~3.5 pixels	KP17-B	~1.05	4750–5600
1990 Nov.....	Tek 1024	432 × 1024	~3.5 e^-	4.5	0.69/pixel	~2.5 pixels	KP007	~1.4	4275–5650

TABLE 2

SPECTROSCOPIC OBSERVING LOG

Object	Other Name	Slit Location	Slit P.A.	Date (1990)	Exposure Time (minutes)
...	NGC 3379	Across center	90°	Feb	10
K46	NGC 750/751	Both galaxies	175	Nov	120
K46-N	NGC 750	North galaxy	85	Nov	100
K99	NGC 1587/1588	Both galaxies	79	Feb	165
K99-W	NGC 1587	Primary galaxy	59	Feb	60
K99-E	NGC 1588	Secondary galaxy	169	Nov	120
K175	NGC 2672/2673	Both galaxies	95	Feb	80
K175-E	NGC 2673	Secondary galaxy	7	Feb	92
K194	NGC 2802/2803	Both galaxies	132	Feb	105
Arp 171	NGC 5718+IC 1042	Both galaxies	104	Feb	150
K564	NGC 7236/7237	Both galaxies	126	Nov	120
K564-SE	NGC 7237	SE galaxy	36	Nov	120

Table 2 provides a log of our spectroscopic observations. When both galaxies were observed in a single setting, the slit was placed across the centers of the two objects. When a single galaxy was observed, the slit was centered on the center of that galaxy.

The exposure time given in Table 2 for a specific object corresponds to the total integration time for all observations of that object. Typically several exposures (ranging from 20 to 60 minutes each) were made at the given location and position angle. These were later co-added.

Before and after each observation we obtained one comparison lamp spectrum (He-Ne-Ar) and one internal lamp flat field. These pairs of exposures bracketed any changes in the wavelength and sensitivity calibrations, respectively, over the course of the observation. Flat-field exposures of the illuminated dome were also taken at the beginning or end of most nights.

Seven radial velocity standard stars were also observed (five in 1990 February and three in 1990 November, with one repeat observation). These were late G and early K stars. Each was trailed along a significant fraction of the slit's length in order to cover the CCD as much as possible. In addition, a frame was taken with a sequence of stellar observations, placing the star at ~ 10 positions along the slit, without trailing. The result was a frame with a series of spectral strips, which was used to calibrate the tilt of the spectra as a function of position along the slit.

2.2. *Spectral Reductions*

The spectroscopic exposures were processed using reduction tasks within IRAF. The sequence of steps followed the usual pattern for long-slit CCD spectral reductions. Bias levels were derived from the overscan strip in each frame and from 10–20 bias exposures taken each night. Object exposures were flat-fielded using illumination-corrected, normalized internal lamp exposures. The wavelength solution for each comparison-lamp exposure was fitted using low-order cubic splines and applied to the corresponding object frame. Each wavelength-calibrated observation was rebinned on a log λ scale for later use by the Fourier Quotient velocity analysis program. The multistrip observations of a star (as described above) were used to correct the tilt of each spectral observation. It was found that the tilt was quite small (~ 1 pixel along the full dispersion direction) and was uniform as a function of slit position. We then had a set of de-biased, flat-fielded, wavelength-calibrated, tilt-corrected two-dimensional spectra. For the galaxies, sky columns were identified, co-added, normalized, and removed from each galaxy column. For the galaxies, individual columns (or pairs or triples, depending on S/N) were extracted as a function of galactocentric radius. For the standard stars, the two-dimensional spectra were collapsed to one dimension by co-adding all of the columns. Each one-dimensional galaxy spectrum was analyzed with Jerry Kriss's FQUOT package, as implemented in STSDAS/IRAF, using each of the standard stars as templates. The final line-of-sight velocity and velocity dispersion at each Galactic position were finally computed from the average of the values obtained from the different template stars.

Observations of NGC 3379 during our 1990 February run provide us with an external check on our velocity derivations. The results are summarized in Table 3, including a comparison with previously published values. We include only recent authors who reported their own redshift and dispersion values. As shown in Table 3, our central velocity dispersion is within 1 σ of each of the published values, and our central redshift is within 2 σ of all except Davies's value. Actually, his Figure 4 indicates a central redshift of 892 ± 28 km s^{-1}, entirely consistent with our central value. His tabulated value and error (which we reproduce here in our Table 3) were derived from a linear fit to the galaxy's rotation curve and hence depend on that extra assumption. We are therefore confident that our velocity measurements for NGC 3379 and for our other program galaxies are accurate and free from any significant systematic errors.

2.3. *Imaging Observations*

We obtained CCD images for the galaxies discussed in this paper at the KPNO #1-0.9 m and 2.1 m telescopes. In most cases, we used the RCA CCD with *B*, *V*, and *R* passband filters. The images were flat-fielded using exposures of the illuminated inside of the dome. Absolute calibrations were obtained by measuring several photometric standard stars throughout the night. The standard star residuals were better than ± 0.05 mag in every case.

In Figure 2 (Plate 3) we show grayscale images of the pairs. The upper panels contain K46, K99, and K175 from left to right, and the lower panels contain K194, Arp 171, and K564 from left to right. These images have been rebinned to similar scales and exposure depths. They represent the equivalent of 900 s red exposures on the 0.9 m telescope and each is approximately 4'.3 on a side. North is up and east to the left in all cases. The image intensity scales were stretched to emphasize the faint outer surface brightness distributions for these pairs,

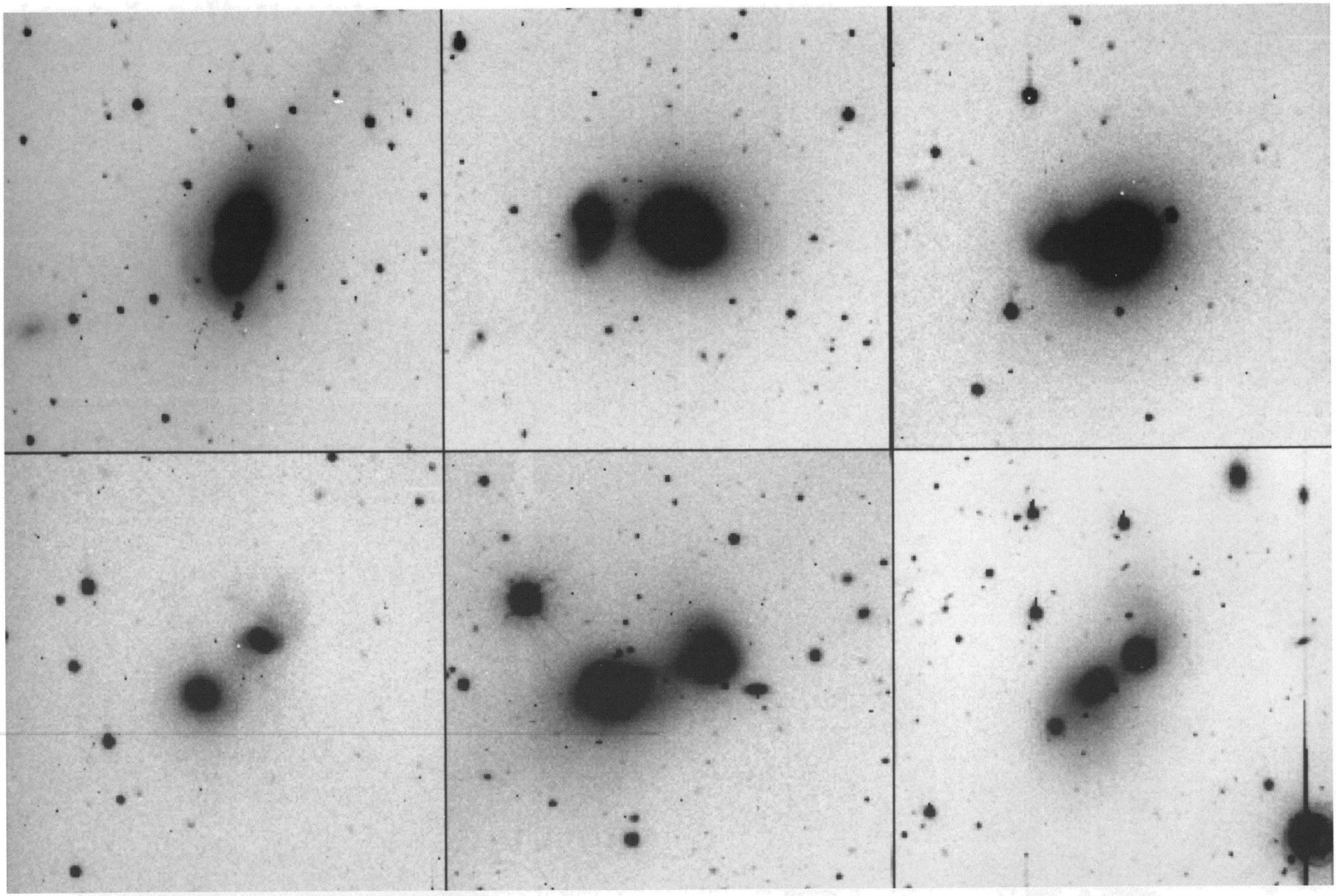

FIG. 2.—Composite grayscale image of the six galaxies studied, drawn from *R*-band CCD images taken at the KPNO 0.9 and 2.1 m telescopes with an RCA CCD (0.″86/pixel). North is up, east to the left. Each picture is 4.′3 on a side. From left to right (starting with the top row): (*a*) K46: NGC 750 (N) and NGC 751 (S). (*b*) K99: NGC 1587 (W) and NGC 1588 (E). (*c*) K175: NGC 2672 (W) and NGC 2673 (E). (*d*) K194: NGC 2802 (NW) and NGC 2803 (SE). (*e*) Arp 171: NGC 5718 (E) and IC 1042 (W). (*f*) K564: NGC 7236 (NW) and NGC 7237 (SE).

BORNE et al. (see 435, 81)

TABLE 3

CENTRAL VELOCITIES AND DISPERSIONS

Galaxy NGC	Source	v_{helio}	Error	σ (km s^{-1})	Error
3379	This work	920	10	233	7
	S + 78	883	18	223	21
	S80	909	13	216	16
	D81	885	5	253	19
	P+87	914	37	204	36
750	This work (P.A. = 175°)	5269	9	209	7
	This work (P.A. = 95°)	5262	9	217	10
	TD81	5220	...	202	29
	D+87	5255	...	216	...
	M91	5220	...	200	...
	W+85	...	...	198	...
751	This work (P.A. = 175°)	5257	10	213	10
1587	This work (P.A. = 59°)	3703	14	218	15
	This work (P.A. = 79°)	3683	18	228	17
	HGVS	3728	10	206	11
	K80	3864	50	...	...
	TD81	3667	22	233	27
	T82	3586	65	...	...
	RC3	3871	34	...	...
1588	This work (P.A. = 79°)	3514	10	159	10
	This work (P.A. = 169°)	3505	5	160	6
	K80	3559	90	...	...
	T82	3516	65	...	...
2672	This work (P.A. = 95°)	4343	10	259	11
	HGVS (P.A. = 95°)	3956	16	258	17
	MK85	4200	...	332	24
	RC3	4255	46	...	...
2673	This work (P.A. = 95°)	3758	6	151	7
	This work (P.A. = 7°)	3765	6	147	7
	HGVS (P.A. = 95°)	3315	10	134	18
	T82	3963	...	...	...
	RC3	3849	46	...	...
	N+90	...	...	175	10
2802	This work (P.A. = 132°)	8736	10	177	16
	W+83	8783	27	189	33
	RC3	8753	34	...	...
2803	This work (P.A. = 132°)	8905	13	213	18
	W+83	8896	37	209	45
	RC3	8854	34	...	...
5718	This work (P.A. = 104°)	8207	12	201	18
	W+83	8259	27	231	26
	RC3	8277	46	...	...
IC 1042 ...	This work (P.A. = 104°)	7997	13	128	20
	W+83	7979	32	176	43
	RC3	7929	46	...	...
7236	This work (P.A. = 126°)	7886	11	232	9
	TD81	7876	21	257	17
	RC3	7855	25	...	...
7237	This work (P.A. = 126°)	7875	17	196	18
	This work (P.A. = 36°)	7892	13	203	13
	TD81	7834	28	225	31
	RC3	7853	23	...	...

SOURCES.—D81 = Davies 1981; D+87 = Davies et al. 1987; HGVS = our previously published HGVS velocities; K80 = Karachentsev 1980; M91 = Madejsky 1991; MK85 = Malumuth & Kirshner 1985; N + 90 = Nieto et al. 1990; P+87 = Prugniel et al. 1987; RC3 = de Vaucouleurs et al. 1991; S+78 = Sargent et al. 1978; S80 = Schechter 1980; T82 = Tifft 1982; TD81 = Tonry & Davis 1981; W+83 = White et al. 1983; W+85 = Whitmore et al. 1985.

sacrificing an accurate display of the higher surface brightness information near the galaxies' centers. Surface brightness data, when combined with velocity and dispersion data, can be used to provide strong constraints on collision models of these pairs, as discussed and demonstrated in previous papers in this series.

Surface brightness contour plots for the pairs are shown in Figure 3, in the same orientation as Figure 2. The faintest contour level represents surface brightness $\approx$23.5 R mag arcsec^{-2}. The interval between the contours is 0.5 R mag arcsec^{-2}. The contours were chosen to reveal the faintest outer structures as well as to show structure at the intermediate brightness levels. The central lower panel shows a small sky level gradient (decreasing counts to the SW) which might in part be due to the presence of a very bright star in the frame.

3. RESULTS

We present in this section the rotation curves and velocity dispersion profiles obtained for the program galaxies. For each pair we describe its morphology and kinematic structure, and discuss its dynamical state. For those systems for which we had obtained HGVS velocities, we overplot those against the new data. A zero-point velocity shift has been applied to the HGVS velocities where necessary to improve the overlap between the velocity curves. No shifts have been applied to the dispersions.

The heliocentric velocities and the velocity dispersions for the centers of each galaxy are listed in Table 3. The centers are defined by the pixel closest to the luminosity peak of each galaxy. Internal consistency of our own results has been checked by computing, for the five galaxies for which we have spectra at two position angles, the difference of the two central velocities in units of the root-mean-square of their respective errors. This difference averages to 0.9 for the velocities and to 0.4 for the dispersions. This may indicate that the errors in the dispersions given by the Fourier Quotient program may be overestimated for our data set.

Table 3 also lists velocities and dispersions drawn from the literature for our sample galaxies. No major discrepancies exist between our results and those previously published. For the NGC 2672/2673 system, our HGVS velocities must have had a zero-point error; for the other systems, the HGVS velocities are in very good agreement with those derived from the new data.

3.1. *NGC 750/751 (Karachentsev 46, Arp 166)*

This classic dumbbell system is a prototype dumbbell pair with isophotes that deviate strongly from pure ellipses (Wirth, Smarr, & Gallagher 1982). It has recently been examined in detail by Madejsky (1991). The two components (Fig. 3) show asymmetric isophotes and a pronounced isophotal twist. Note the relatively straight sharp isophotes on the east and southeast sides. A broad, straight tail is visible at very faint levels extending to the NW, all the way to the edge of the frame (P.A. = 30°). Also note the shell-like structure surrounding the pair (Fig. 2). The narrow feature extending to the south side of this pair is a defect in this particular RCA CCD.

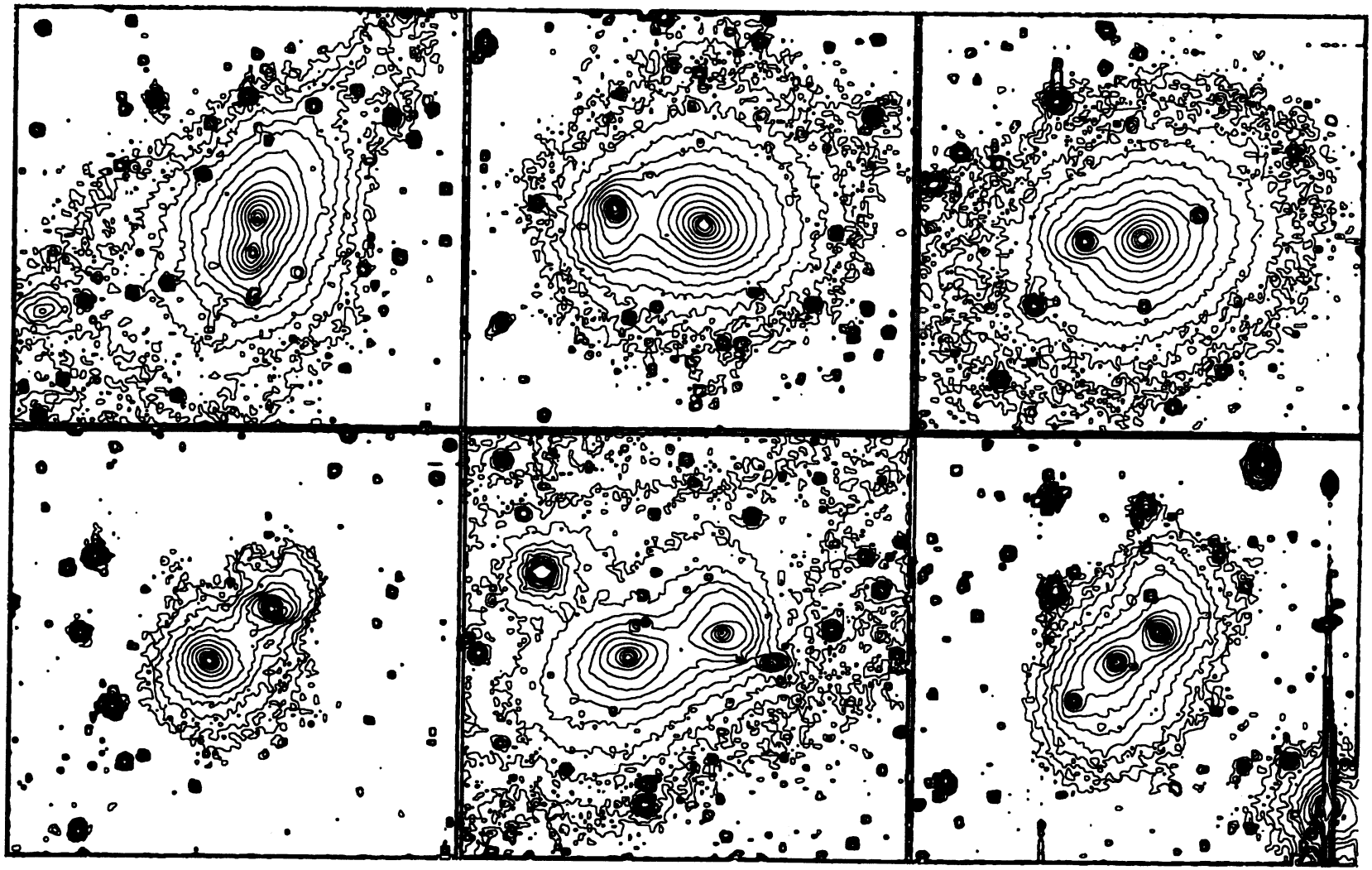

FIG. 3.—Isophotal contour plots of the six galaxies studied, drawn from *R*-band CCD images taken at the KPNO 0.9 m telescope with an RCA CCD (0.″86/pixel). North is up, east to the left. Contours are separated by 0.5 *R* mag arcsec^{-2}. From left to right (starting with the top row): (*a*) K46: NGC 750 (N) and NGC 751 (S). (*b*) K99: NGC 1587 (W) and NGC 1588 (E). (*c*) K175: NGC 2672 (W) and NGC 2673 (E). (*d*) K194: NGC 2802 (NW) and NGC 2803 (SE). (*e*) Arp 171: NGC 5718 (E) and IC 1042 (W). (*f*) K564: NGC 7236 (NW) and NGC 7237 (SE).

Madejsky (1991) points out that the inner isophotes have a drop-shape. Because of the similarity of the contact isophote with a Roche-lobe surface, it is tempting to propose a stable, circular binary orbit configuration for NGC 750/751, and for other dumbbells with drop-shape isophotes. Indeed, Rix & White (1989) use NGC 750/751 as a prototype for models of equilibrium configurations for binary galaxies in circular orbits. As Wirth et al. (1982) point out, detailed velocities and isophotal shapes are needed before the connection between drop-shape isophotes and circular orbits can be made (we carry out this type of analysis for the NGC 4782/4783 system, in Paper V, which leads in that case to discarding the circular orbit hypothesis). For NGC 750/751, the morphology gives clues against a circular orbit interpretation. The straight, low-surface brightness tail is surely of tidal origin. Tidal tails are transient features, which indicates that the pair has undergone a recent close collision, or that it is on a highly elliptical orbit. To the SE, the outer isophotes are distended, probably due to tides as well.

We took two spectra, one along the line joining the two nuclei (P.A. = 175°) and another along the perpendicular direction centered on the bigger, northern component (NGC 750). Figure 4*a* shows the velocity and velocity dispersion profiles for the spectrum at P.A. = 175°; Figure 4*b* shows those for P.A. = 85°. NGC 750 (north component) is a slow rotator along both position angles, with velocities slightly increasing to the south and to the west. In contrast, NGC 751 (southern component) shows rapid rotation; line-of-sight velocities change by 230 km s^{-1} over 10″. The velocity curve shows an abrupt downturn at 6″ south of the nucleus, and an abrupt upturn at 4″ north of the nucleus. This peculiar S-shape velocity curve is a form of double U-shape rotation pattern (§ 4). It is most likely a transient state resulting from the interaction with NGC 750. We investigated in detail the response of a rotating galaxy to a strong tidal field in Paper VI. We found that, for a perturber field moving with inclination $i = 90°$ with respect to the plane of the rotating galaxy, and with argument of pericenter $\omega = 0°$, a pole-on view of the system resulted in an S-shape rotation curve in the secondary (see Fig. 11 of Paper VI, second panel). In the NGC 750/751 system, the central velocities for the two galaxies are nearly identical (Table 3), which indicates that the three-dimensional relative velocity is almost orthogonal to the line of sight (i.e., that we have a nearly pole-on view of the binary orbit). Our models of Paper VI then suggest that the velocity curve of NGC 751 beyond the central 5″ has been perturbed by the tidal field of NGC 750, and that we are seeing NGC 751 nearly edge-on. Such a coherent response in NGC 751 indicates a high degree of order in its internal motions; this galaxy may therefore be an S0 rather than an elliptical. Because of the rapid rotation of NGC 751, we infer that the straight tail to the NW of the system originates in the southern side of NGC 751 and bends around to the NW; an origin in the northern component NGC 750 is unlikely, as the latter rotates slowly.

The velocity dispersion profiles show local minima at the locations of the two galaxy nuclei, providing further evidence for the presence of U-shaped dispersion profiles in interacting ellipticals (see § 5). In a region 15″ wide between the nuclei, dispersions increase by about 70 km s^{-1}. Madejsky (1991) shows that such an increase cannot be explained as the result of superposition of two undisturbed velocity distributions with different mean velocities, and thus it provides evidence for dynamical heating.

The pair NGC 750/751 shows the most unusual velocity dispersion profile in our sample. Dispersions show alternating maxima and minima as one moves outward from the center of each galaxy in the direction away from the companion (Fig. 4). The symmetry of this pattern is most unusual if we note that the velocity fields of the two galaxies are very different (rapid rotation versus no rotation). This peculiar dispersion pattern might provide strong diagnostics to discern between equilibrium models and collision models for this system.

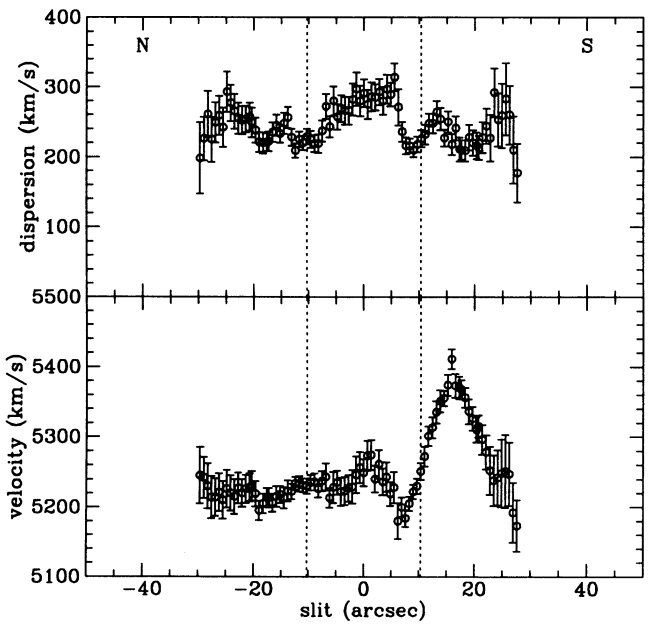

FIG. 4*a*

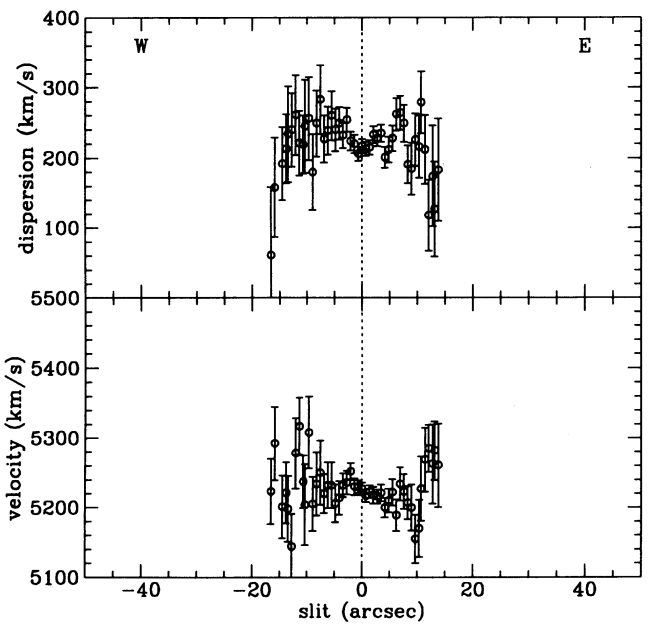

FIG. 4*b*

FIG. 4.—Velocity and dispersion curves for the NGC 750/751 (K46) pair. All velocities are heliocentric. The galaxy centers are indicated by the vertical dashed lines. Position angles are measured north through east. (*a*) Along P.A. = 175° (includes both galaxies). (*b*) Along P.A. = 85° (NGC 750).

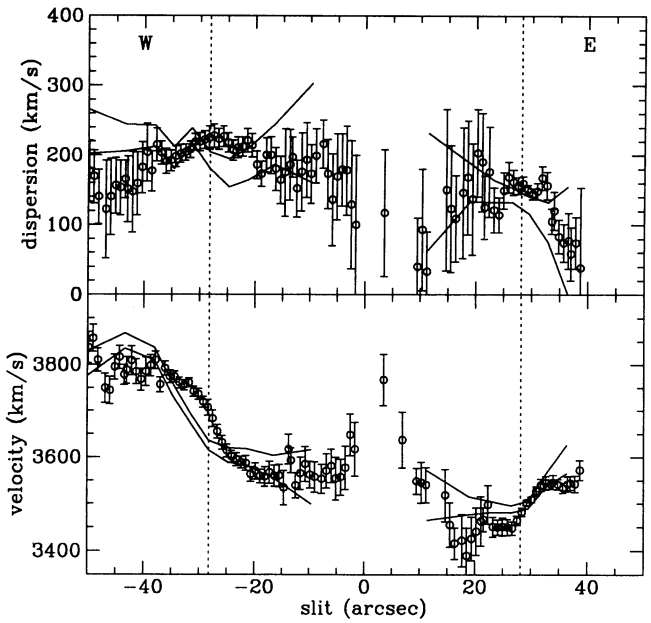

FIG. 5a

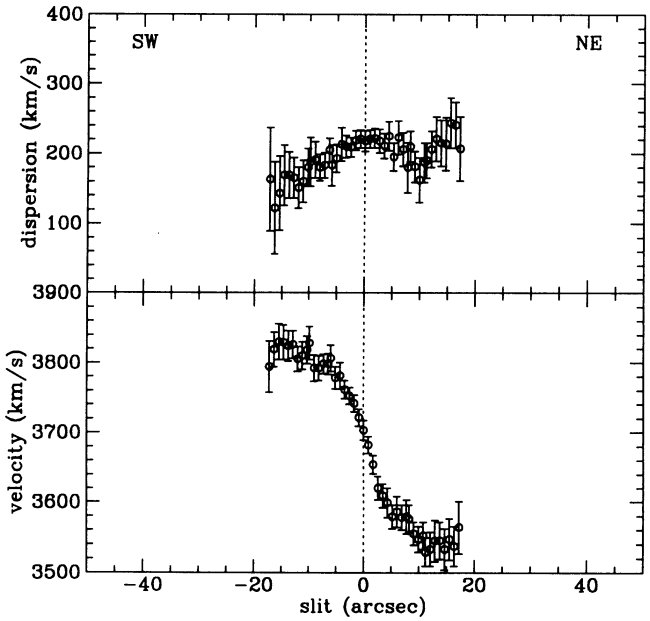

FIG. 5b

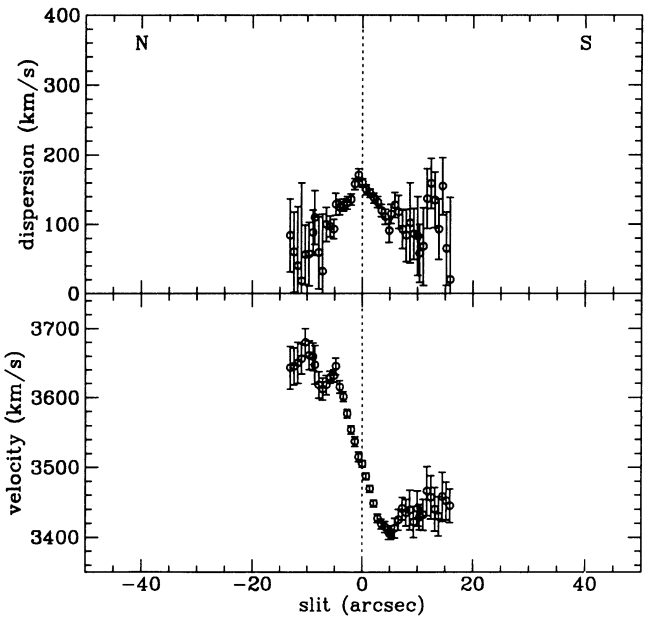

FIG. 5c

FIG. 5.—Velocity and dispersion curves for the NGC 1587/1588 (K99) pair (see caption to Fig. 4). (*a*) Along P.A. = 79° (includes both galaxies). (*b*) Along P.A. = 59° (NGC 1587 major axis). (*c*) Along P.A. = 169° (NGC 1588 major axis).

Our velocity and dispersion curves generally coincide with those of Madejsky (1991), except that the amplitude of his rotation curve is smaller than ours. This is probably due to the lower spatial and spectral resolutions of his observations, which would have a significant effect on the measured line-of-sight velocities precisely in those regions where the velocity is changing rapidly (as in NGC 751). We agree with Madejsky's analysis of the system: the NW tidal tail and the distorted kinematics of NGC 751 suggest that the NGC 750/751 pair is in the midst of a collision and are inconsistent with a stable or semistable configuration for the system. Numerical simulations will help to place additional dynamical constraints on the state of this interesting system.

3.2. *NGC 1587/1588 (Karachentsev 99)*

Papers III and IV present velocity data and numerical models for this pair. A surface brightness contour plot is shown in Figure 3. The inner isophotes are distorted by saturation in the CCD. NGC 1588, the larger component of the pair, is an E1 galaxy with minor isophotal distortions. NGC 1588, the secondary, is elongated and shows asymmetric outer isophotes. These distortions were shown in Paper IV to be of tidal origin. The new observations described in this paper were aimed at checking the validity of the numerical models presented in Paper IV, by measuring velocities along new slit orientations. We present new velocity data taken along the line connecting the nuclei (P.A. = 79°, Fig. 5*a*), along the major axis of NGC 1587 (P.A. = 59°; Fig. 5*b*), and along the major axis of the secondary NGC 1588 (P.A. = 169°; Fig. 5*c*).

NGC 1587 is a rapid rotator. Along the major axis (P.A. = 59°) the line-of-sight rotation reaches 146 km s^{-1}, which implies a rotation parameter $V/\sigma_0 = 0.67$, and $(V/\sigma_0)^* = 1.34$. Rotation along P.A. = 79° is somewhat lower: $V = 116$ km s^{-1}. The velocity dispersion profile peaks at the center and gently drops outward. Along the major axis, beyond 10″, dispersions increase outward in the direction toward NGC 1588, probably due to tidal heating.

The secondary NGC 1588 is a rapid rotator as well. The velocities in Figure 5*c* imply $V/\sigma_0 = 0.73$ along the direction of the tail. The velocity curve appears regular inward of 5″, and irregular outward. Note that, along the line connecting the two nuclei, the rotation curve is not symmetric with respect to the luminosity peak of the galaxy. Thus, despite its resemblance to the rotation curves of isolated galaxies, the velocity curve of NGC 1588 does not describe equilibrium rotation but probably an effect of the tidal perturbation. The dispersion profile is single-peaked along P.A. = 169° and double-peaked along P.A. = 79°.

Figure 5*a* shows that the agreement between the velocity data presented here and the old data presented in Paper III is acceptable, though not perfect (particularly in the spatial direction). A vertical offset of $+100$ km s^{-1} has been applied to the HGVS data before plotting, but no offset is allowed in the horizontal (spatial) direction since the galaxy centers were defined in all cases to be at the peak surface brightness along the spectroscopic slit. Thus the slight mismatch between horizontal scales for the two data sets cannot be easily resolved. It is most probably the result of an inaccurate spatial scale being used for the HGVS velocity data, but we cannot prove this with the available information.

3.3. *NGC 2762/2763 (Karachentsev 175, Arp 167)*

For this very unequal pair (Figs. 2 and 3), two low surface brightness plumes in the secondary provide photometric evidence for an interaction. We studied this system in Paper VI. The velocity data presented in that paper show a large velocity difference between the two galaxies, and a U-shaped rotation profile in the secondary. After numerical modeling, we argued that, in order to generate the plumes in the secondary, the latter had to be a rotating galaxy, despite the fact that no rotation was detectable along the slit in our HGVS data. We concluded that the galaxy had to rotate in a direction nearly orthogonal to the slit. Here we present velocity data along the line connecting the two nuclei, to check the U-shaped rotation profile in the secondary, and along an orthogonal direction centered on the secondary, to verify the prediction of our models that NGC 2673 should rotate. We show these rotation curves in Figures 6*a* and 6*b*, respectively. Figure 6*a* shows that the primary NGC 2672 (west component) has no rotation along the slit and has a flat velocity dispersion profile. Along this position angle, the secondary NGC 2673 (east component) does not rotate but shows a weak U shape, in agreement with the old data. Along P.A. = 7° (Fig. 6*b*), the secondary does actually rotate, with an amplitude of 53 km s^{-1}, north receding. This confirms the prediction we made in Paper VI that NGC 2673 would show rotation along this direction (see § 4).

The HGVS data (solid lines in Fig. 6*a*) agree quite well with the new CCD data presented here (except for a slight horizontal mismatch in the spatial scale, which is probably a problem with the HGVS scale, as mentioned above for the NGC 1587/1588 velocity profile). An offset of $+510$ km s^{-1} in the recession velocities had to be applied to the HGVS velocities in order to produce the match shown in Figure 6*a*; our new velocities are closer to determinations by other authors (see Table 3 and Paper VI) and are probably correct. The U-shaped dispersion profile seen in the HGVS data for the secondary does not appear in the new data. Rather, we see a small central peak plus a (possible) upturn 3″ from the center. For some lines of sight between the two galaxy centers, the line-of-sight distribution of velocities must be double-peaked. We verified this by examining the velocity cross-correlation between the galaxy and template stellar spectra. For these regions, the Fourier Quotient program computes an abnormally high dispersion that has little physical meaning. Consequently, we excluded those points from the plots in Figure 6*a*.

3.4. *NGC 2802/2803 (Karachentsev 194)*

A surface brightness contour plot of this system is shown in Figure 3. The NW component (NGC 2802) shows a pronounced isophotal twist, a broad, low surface-brightness luminosity extension to the NW and a thinner low surface-brightness tail to the NE; the latter, together with a less prominent tail to the SW (barely visible on our figures), draws a Z-shaped pattern across the nucleus. The Z-shaped pattern and the strong isophotal twist are expected effects in the tidal interaction of a rapidly rotating, flattened galaxy. Therefore, we suspected that NGC 2802 should rotate rapidly, or that it should contain a rapidly rotating subsystem. To verify this, we

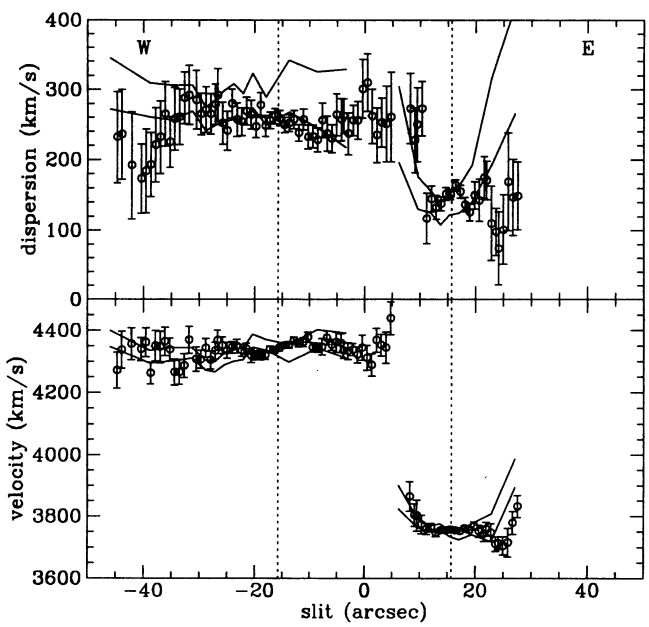

FIG. 6*a*

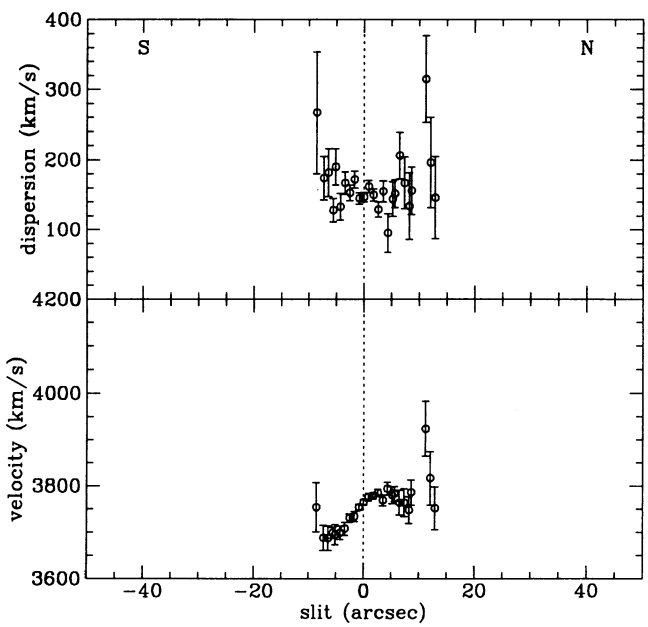

FIG. 6*b*

FIG. 6.—Velocity and dispersion curves for the NGC 2672/2673 (K175) pair. (See caption to Fig. 4.) (*a*) Along P.A. = 95° (includes both galaxies). (*b*) Along P.A. = 7° (NGC 2673).

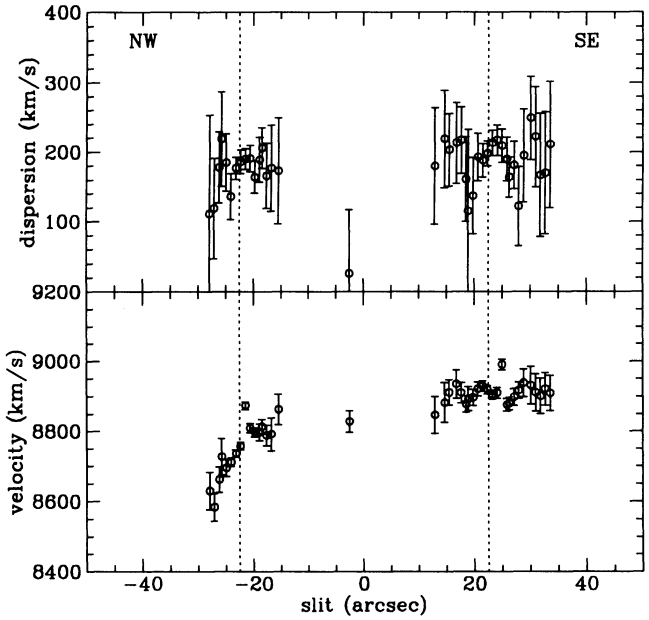

FIG. 7.—Velocity and dispersion curves for the NGC 2802/2803 (K194) pair along P.A. = 132° (includes both galaxies) (see caption to Fig. 4).

took spectra along the line connecting the two nuclei. The velocity results are shown in Figure 7. Indeed, we see that NGC 2802 is a rapid rotator, with a rotation velocity along the galaxy's major axis that is probably much higher than the velocities that we measured (not along the major axis). Our rotation curve is highly asymmetric with respect to the galaxy's luminosity center. NGC 2803 (SE component) shows no rotation along the slit and a dispersion profile which declines with radius. Near the center of each galaxy we find a highly deviant velocity value. We do not believe these values to be real; they probably originate in poorly subtracted cosmic rays that happen to exist at each of these two positions.

The two types of tidal distortions seen in NGC 2802 (the NW fan plus the thin tails) suggest that this galaxy might be a composite system, maybe an S0 or an elliptical with an embedded disk. That the tails are faint and short lends support to the latter of these possibilities. In fact, Rix & White (1990) suggest that small disks could account for ~20% of the light in most elliptical galaxies. Therefore, these disks could contribute to the thin tidal features occasionally seen in encounters between ellipticals. In NGC 2802, such a disk appears to be revealed by its response to the interaction with NGC 2803.

3.5. *NGC 5718/IC 1042 (Arp 171)*

The Arp 171 pair represents the brightest two galaxies in the poor cluster MKW8 (Morgan, Kayser, & White 1975), where the third-brightest galaxy is very much fainter than these two; it is unlikely that the pair is dynamically affected by the small number of significantly fainter companions in the group.

The pair shows strongly distorted isophotes, with the orientation rotating strongly with decreasing surface brightness (Fig. 3). Based on our previous experience trying to model such systems as superpositions of normal galaxies, we would posit that there is no way that this pair can be such a superposition. Of particular note are the strong tidal distensions toward the NNE in the west member and toward the SE in the east member.

This pair has been ignored in most studies of binary galaxies, yet it is a fine example of a dumbbell with strongly distorted morphology, more so than the prototype NGC 750/751 (§ 3.1). Both components show isophotal distortions at low and high surface brightness levels, in such a way that the sense of the compression/distension of isophotes changes with isophotal level (Fig. 3). The isophotes near the critical, or contact isophote, show a drop-shape morphology similar to that of NGC 750/751, but the deviation from ellipticity is much stronger in the Arp 171 pair. In NGC 5718 (the east galaxy), the isophotes approach a diamond-shape. For both galaxies, some isophotes show noticeable straight segments.

We took one spectrum along the line connecting the galaxy nuclei. The velocity results (Fig. 8) show that the rotation curves are featureless, and that both galaxies do not rotate along the slit. The broad plume protruding out of IC 1042 suggests however that this galaxy may rotate along a direction perpendicular to the slit, as coherent responses require coupling of the orbit to organized internal motions (Paper VI). The central dispersions are unusually different given that the two components have similar sizes (Fig. 3). Assuming that the luminosities scale as the fourth power of the velocity dispersions, our reported dispersions would imply a luminosity ratio of 6, while the dispersions quoted by White et al. (1983) would imply a luminosity ratio of 3. However, the photometric luminosity ratio is approximately 1.6. Two explanations are possible for this discrepancy. Either a fraction of the mass in IC 1042 may be rotationally supported (i.e., forms a disk, so that the central dispersion corresponds to that of a central bulge of lower mass), or the dispersion in NGC 5718 may be higher as a result of the interaction, thus being indicative of a nonequilibrium state. The first hypothesis seems less plausible given the lack of detectable rotation in either of the two galaxies, but, as we said above, this galaxy may rotate along a direction perpendicular to our chosen slit position angle. Dynamical modeling of the binary interaction should help to elucidate this question.

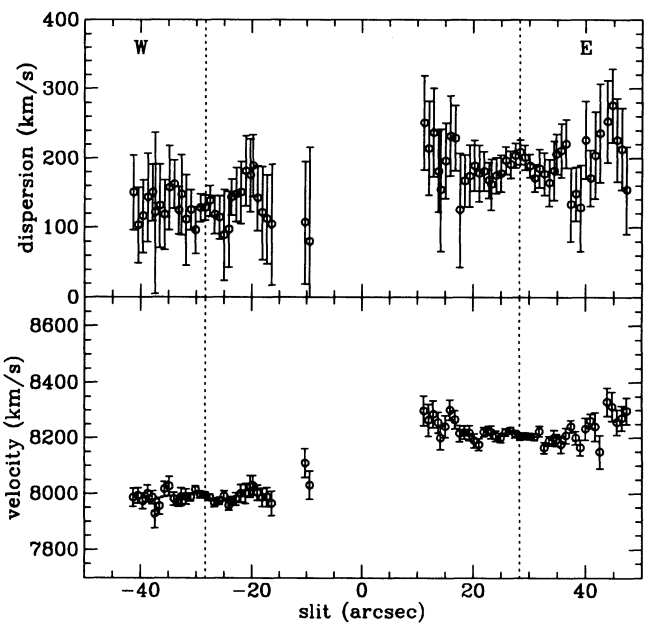

FIG. 8.—Velocity and dispersion curves for the NGC 5718/IC 1042 (Arp 171) pair along P.A. = 104° (includes both galaxies) (see caption to Fig. 4).

3.6. *NGC 7236/7237 (Karachentsev 564)*

This pair was previously studied in detail by us. Surface photometry and kinematic data were presented in Paper III, with numerical models of the collision between the two galaxies in Paper IV. We show a surface brightness contour plot of the system in Figure 3. For both galaxies the isophotes are more distended on one side than on the other. This pattern of distortions is typical of interacting ellipticals, as we have shown in previous papers in this series. The NW component is highly flattened in its central parts, and the kinematic data in Paper III indicate that this galaxy rotates rapidly, at least in its central parts. We took spectra of this system along the line connecting the galaxy nuclei (P.A. = 126°), and along the perpendicular direction centered on the SE component NGC 7237. The velocity results are shown in Figures 9*a* and 9*b*, respectively. Figure 9*a* shows that the NW component, NGC 7236, indeed rotates rapidly. Note that the slit lies along the shortest isophotal axis of this galaxy. This rapid rotation supports the suggestion in Paper III that this galaxy is in fact an S0. The SE component, NGC 7237, also rotates at the core, albeit with lower amplitude. No rotation is detected in NGC 7237 along the perpendicular direction (Fig. 9*b*). The velocity difference between the galaxy centers is 22 km s^{-1}, indicating that the three-dimensional relative velocity of the pair is nearly perpendicular to the line of sight. The central velocity dispersion is higher for the NW component, although the two galaxies have similar sizes and luminosities (Paper III). The solid lines in Figure 9*a* represent the velocity results obtained with the HGVS (mean $\pm 1\ \sigma$). The velocities agree within the errors, while the HGVS dispersions are systematically lower.

4. COMPARISONS WITH COLLISION MODELS

In this section we compare our new kinematic data with our published collision models for K99 (§ 4.1), K175 (§ 4.2), and K564 (§ 4.3). In particular, we draw attention here to the comparisons between those models' predictions and the new rotation and dispersion profiles measured along previously unobserved position angles. The models were derived from comparisons with our previous HGVS data, and so these new data provide an independent check on the validity of the models.

4.1. *NGC 1587/1588 (K99)*

We reported in § 3.2 on new measurements of the rotation and dispersion velocity profiles along the line connecting the centers of the two galaxies in K99. The HGVS version of these velocities (Paper III) was the only kinematic data set used in Paper IV to constrain the collision model for K99. We find that the published model velocities indeed match the new velocity curves quite well (Fig. 10); the dispersion profile matches particularly well. There are two minor discrepancies in the rotation profile. First, the primary galaxy (whose velocities appear at positive projected radii in Fig. 10) is rotating faster than in our model. We pointed out in Paper III that this galaxy (NGC 1587) is a very rapid rotator, significantly faster than other galaxies with its flattening (E2) and also faster than our initial galaxy model would allow. So, we are not surprised by this minor deviation of our model from the new observations. Second, the secondary galaxy (whose velocities appear at negative projected radii in Figure 10) has a small amount of retrograde rotation. This was not evident in our previous low-S/N HGVS data, and so we did not even attempt to include such rotation in the collision model of Paper IV. The mismatch here is thus not a concern.

The major axis of NGC 1587 is rotated by 20° from the position angle of the line of centers. Given the rapid rotation in this galaxy, we chose to measure its rotation and dispersion velocities along its major axis. These are shown in Figure 11, with the collision model predictions shown as two solid lines (mean velocity $\pm\ 1\ \sigma$). Again we see the agreement between the model and observed dispersion profiles.

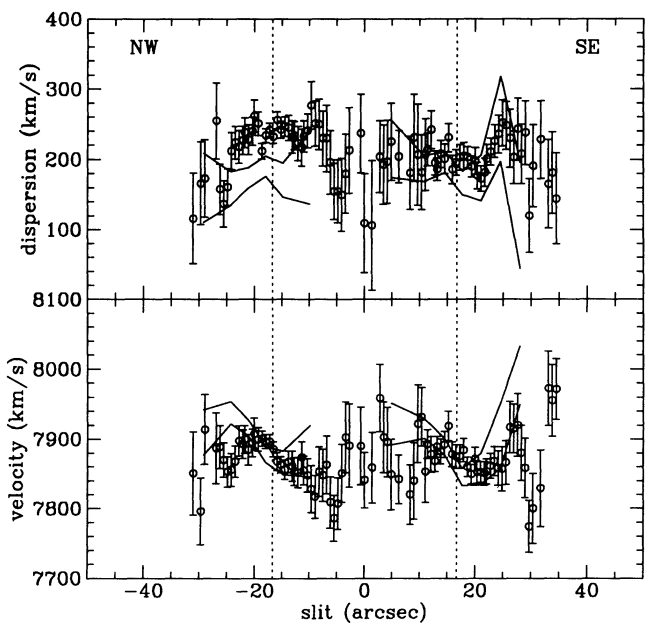

FIG. 9*a*

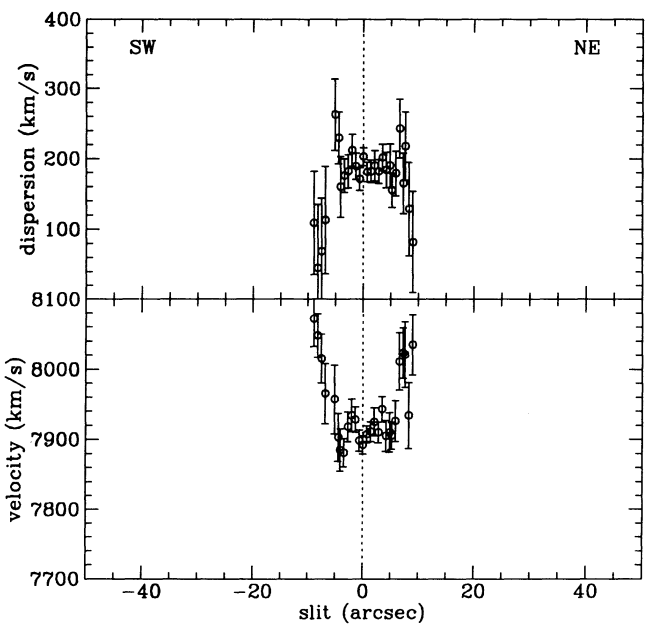

FIG. 9*b*

FIG. 9.—Velocity and dispersion curves for the NGC 7236/7237 (K564) pair (see caption to Fig. 4). (*a*) Along P.A. = 126° (includes both galaxies). (*b*) Along P.A. = 36° (NGC 7237).

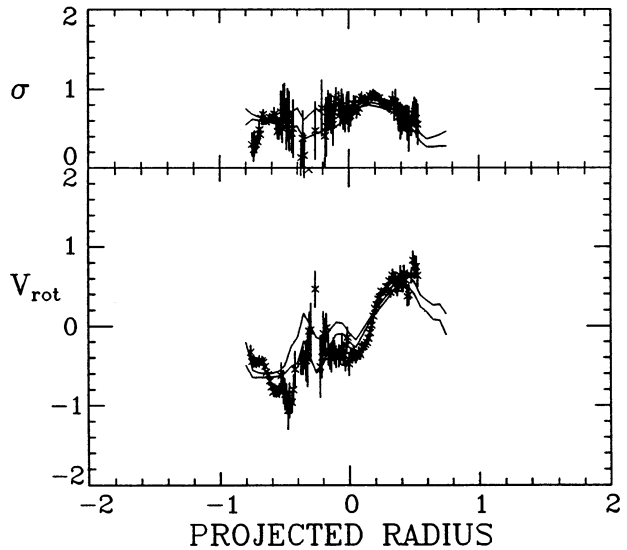

FIG. 10.—Kinematic data for K99 binary, along the line connecting the galaxies' centers (P.A. = 79°), are plotted as points with error bars. Collision model velocities (Paper IV) are plotted as two solid lines (mean ± 1 σ). East is to the left. The rotation profile is shown in the lower panel; the dispersion profile in the upper panel.

We measured velocities at one other location in the K99 pair as a further test of our collision model: along the tail in the secondary galaxy (NGC 1588). The rotation and dispersion profiles are shown in Figure 12 along with the collision model predictions. It is quite clear from this that our model is deficient in having no rotation in the secondary galaxy. We could have introduced rotation in the model to account for the tail but decided not to do so for two reasons: (1) a short tidal tail was formed by simple tidal heating, and (2) we had no evidence of rotation in the HGVS data. We thought that these were sufficient reasons to exclude rotation in this galaxy. But, if we had included rotation in this galaxy, it would have made the model more robust: producing a longer, more distinct tidal tail, in agreement with the observed morphology. That is, the

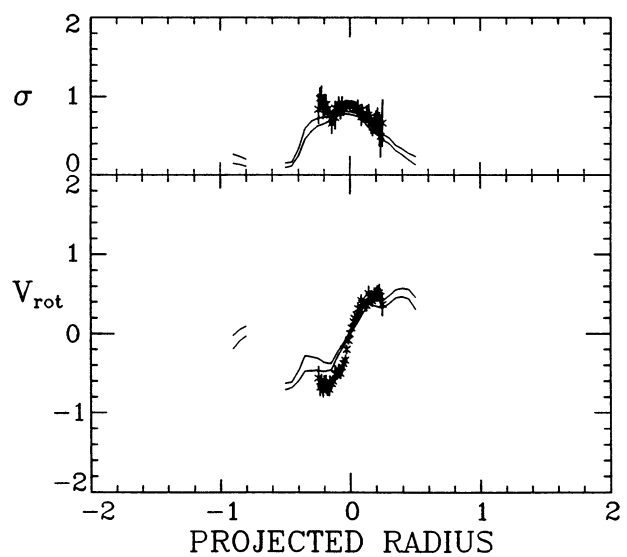

FIG. 11.—Kinematic data and collision model velocities along the major axis (P.A. = 59°) in NGC 1587 (K99 primary). East is to the left.

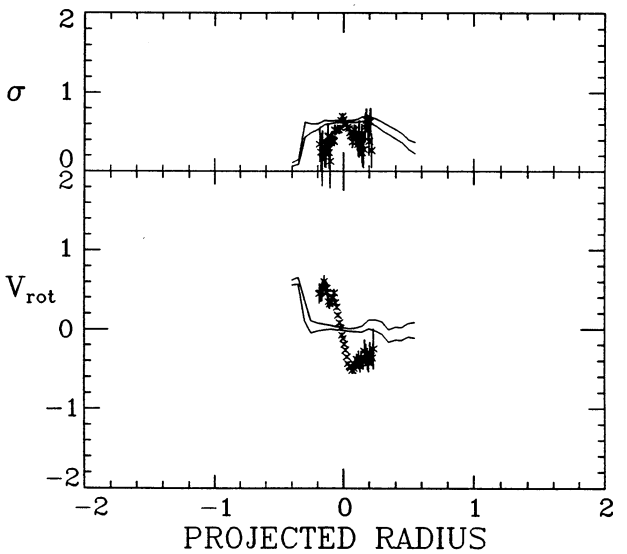

FIG. 12.—Kinematic data and collision model velocities along the tidal tail (P.A. = 169°) in NGC 1588 (K99 secondary). South is to the left.

model morphology is more like a distended tidal lobe (aspect ratio of unity) than a tidal tail (aspect ratio of 2:1, as actually observed). In hindsight, we realize now that we should have predicted that rotation would be necessary to account for the "thin" tail morphology. In addition, Davies et al. (1983) have shown that faint ellipticals do have greater rotation rates than brighter ellipticals, and so we could have naturally included an appropriate degree of rotation in our model for this particular galaxy. Thus, we do not consider the mismatch in the rotation curve of Figure 12 to be a failure of our collision model, but it represents an improvement in our knowledge of this system and a verification of our physical model for tail formation (Borne & Richstone 1991; McGlynn & Borne 1991, and references therein). The differences between the model and observed dispersion profiles in Figure 12 are likewise a consequence of the fact that the real galaxy is more rotationally supported, with velocity dispersion consequently decreasing as a function of radius, whild the model galaxy is dispersion-supported out to large radii.

4.2. *NGC 2672/2673 (K175)*

We reported in § 3.3 on new measurements of the rotation and dispersion velocity profiles along the line connecting the centers of the two galaxies in K175. The HGVS version of these velocities was the only kinematic data set used in Paper VI to constrain the collision model for K175. We find that the published model velocities indeed match the new velocity curves very well (Fig. 13).

We measured velocities at one other location in the K175 pair as a particularly strong test of our collision model: in the secondary galaxy (NGC 2673) along a line orthogonal to the line of centers. The rotation and dispersion profiles are shown in Figure 14 along with the collision model predictions. We see that not only does the galaxy rotate, but it rotates in the right sense at the very center of the galaxy, and also the tidal heating and superposition effects are also well modeled. This is very gratifying because we had no previous evidence in the HGVS kinematic measurements that this galaxy was rotating at all. We determined from our modeling efforts for this system that a certain degree and orientation of rotation in NGC 2673 was

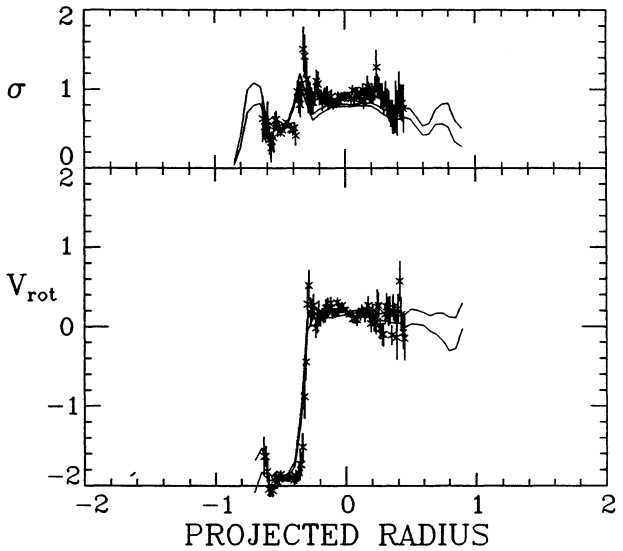

FIG. 13.—Kinematic data and collision model velocities along the line connecting the galaxies' centers (P.A. = 95°) in the K175 binary. Collision model velocities (Paper VI) are plotted as two solid lines (mean ± 1 σ). East is to the left. The rotation profile is shown in the lower panel; the dispersion profile in the upper panel.

required by the morphology. This was a strong prediction of that model (Paper VI). It is also consistent with the results of Davies et al. (1983) for rotation in faint ellipticals. It is quite clear from Figure 14 that our collision model has been vindicated: NGC 2673 does indeed rotate, in the correct sense, and with the correct amplitude. No evidence for this rotation existed prior to these observations other than that deduced from our models.

4.3. *NGC 7236/7237 (K564)*

We reported in § 3.6 on new measurements of the rotation and dispersion velocity profiles along the line connecting the centers of the two galaxies in K564. The HGVS version of these velocities (Paper III) was the only kinematic data set used in Paper IV to constrain the collision model for K564. We discovered during the analysis of our new CCD velocities that in Papers III and IV we had in fact inverted the spatial coordinates of the HGVS velocities for K564. This $x \rightarrow -x$ inversion has been corrected in all of the results presented in this paper. Apart from having east and west reversed in Paper III, this error did not affect the observational results discussed in that paper. However, this parity flip does affect our chosen collision model (Paper IV). Fortunately, since the two galaxies have nearly identical luminosities, line-of-sight velocity profiles, and velocity dispersion profiles, and since the orbit of the pair is viewed nearly pole-on, the system is roughly degenerate under southeast-northwest reflection, and therefore our mistake (which was masked by this degeneracy) had fortuitously little affect on the orbital parameters of our collision model presented in Paper IV. However, what does need to change in that model is the sense of rotation (i.e., the direction of the rotation axes) for the two galaxies. When we make this parity inversion, we find a collision model that still matches the morphological and kinematic data for this system very well. This is demonstrated in Figure 15, where we plot the modified model velocities against the new observed velocities. The good match between model and observation is gratifying.

We measured velocities at one other location in the K564 pair as a further test of our now-modified collision model: along the minor axis in the SE component (NGC 7237). The rotation and dispersion profiles are shown in Figure 16 along with the new collision model predictions. Where there is observational data to make the comparison, we see that the dispersion profile is well matched and that the rotation curve is only marginally so. In particular, the northeast wing of the rotation profile is satisfactorily matched, while the southwest wing deviates between model and observation in the sign of the rotation. This is a case where the data actually show evidence for a U-shaped rotation profile and the model does not. It is not clear if this discrepancy is a result of our choice of initial galaxy

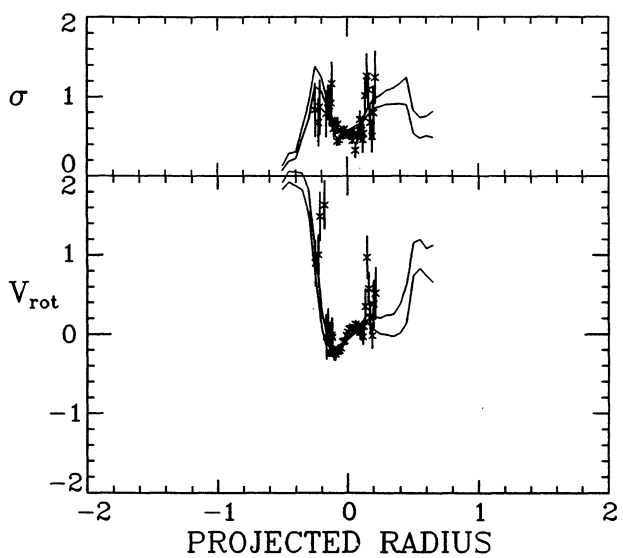

FIG. 14.—Kinematic data and collision model velocities in NGC 2673 (K175 secondary) along a line orthogonal to the line of centers (P.A. = 7°). South is to the left.

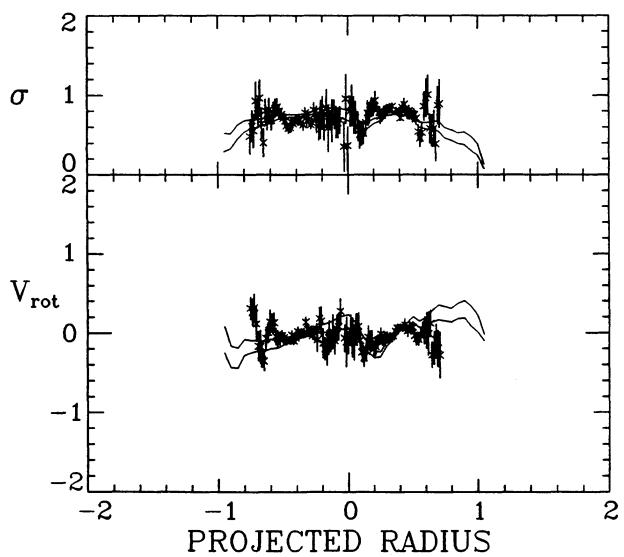

FIG. 15.—Kinematic data and collision model velocities along the line connecting the galaxies' centers (P.A. = 126°) in the K564 binary. Collision model velocities (Paper IV) are plotted as two solid lines (mean ± 1 σ). Southeast is to the left. The rotation profile is shown in the lower panel; the dispersion profile in the upper panel.

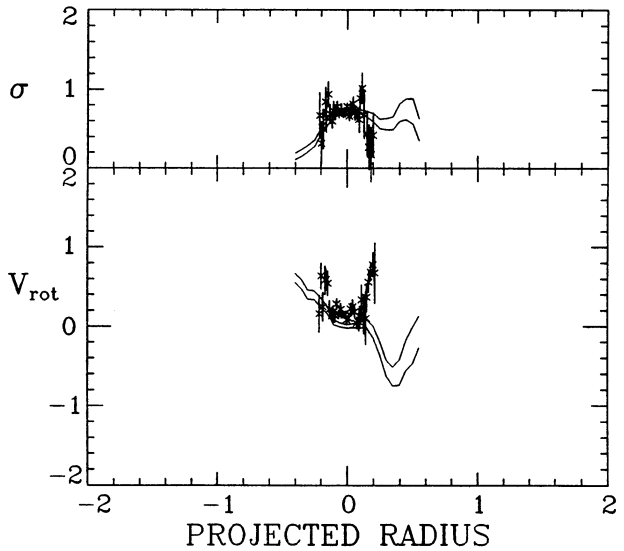

FIG. 16.—Kinematic data and collision model velocities along the minor axis (P.A. = 36°) in NGC 7237 (SE component of K564). Northeast is to the left.

density profile or rotation profile, or if it results from using the wrong collision model (as described above). Given the good match between the optical morphology of the pair and the kinematics along the line of centers, we believe that the collision model is probably okay and that the details of the initial model for NGC 7237 is likely to be the root cause of the observed deviations in Figure 16. We argued in Paper IV that those internal galaxy parameters were less constrained by the data and should consequently match less well.

5. U-SHAPED VELOCITY AND VELOCITY DISPERSION PROFILES

The data presented here provide evidence for the presence of U-shaped rotation curves in interacting elliptical galaxies (§ 1). We confirm the existence of these patterns, but modify slightly the picture as we described it in previous papers in this series. In the earlier data (reproduced in Fig. 1), the galaxy nucleus was typically found to lie at a local extremum of the rotation curve. In the new data, while the rotation curve does again show a turn-around near the center, the extremum appears at a finite distance from the nucleus. Of the 12 galaxies studied, four show such U-shaped rotation curves: NGC numbers 751, 2673 (P.A. = 7°), 7236 (inverted U), and, with lesser significance, NGC 7237 (see Figs. 4–9).

NGC 1588 has a rotation curve which does not turn around, but which is strongly asymmetric (Fig. 5*a*); this pattern may be generated by the same process which creates U-shaped rotation curves. In NGC 751, 2673, and 7236, the rotation is normal out to some radius, then turns around. In Paper III, we described the relation of U-shaped rotation profiles to tidal coupling in interacting elliptical galaxies. It was argued that tidal coupling in ellipticals with no net rotation will result in U-shaped rotation profiles with the galaxy nucleus at the base of the U. An extension to that discussion would suggest that when the galaxy has a small degree of internal rotation, as do some of the galaxies in our sample, tidal coupling should produce the types of perturbed profiles seen in our data. That is, a rotation curve that is undisturbed at small radii will turn over at a moderate distance (i.e., a few kpc) from the center of the galaxy as a result of a similar tidal coupling.

While interactions do generate U-shaped rotation profiles, such profiles do not always trace the effects of an interaction. Light superposition cannot be excluded without detailed modeling of the contributions of the two galaxies to the light along the line of sight. One example of this ambiguity is NGC 751; following Madejsky (1991), light contamination from NGC 750 might start affecting the velocities measured in NGC 751 at about 5″ from the galaxy nucleus on the side nearest to NGC 750. Since the rotation curve does in fact turn around at 4.″1 north of the NGC 751 nucleus (Fig. 4*a*), superposition effects cannot be strictly ruled out. However, such a sharp upturn in the velocity curve (at abscissa = 5″) is unlikely to result from superposition, and it suggests a dynamical effect. The downturn at abscissa = 15″ is also a form of (inverted) U shape, almost certainly originating in the interaction.

U-shaped *dispersion* profiles are seen in many of the galaxies studied. From the results of § 3 we find that eight out of the twelve galaxies show U-shaped (or similar) dispersion profiles. These are NGC numbers 750, 751, 1588, 2673, 5718, 7236, 7237, and IC 1042. Therefore, the new data confirm our earlier result derived from lower signal-to-noise HGVS spectra: U-shaped velocity dispersion profiles are common in strongly interacting elliptical galaxies (see also Madejsky 1991; Madejsky et al. 1991; Bender et al. 1991). It is most clear that dispersions rise outward on the side of the galaxy farthest away from the companion galaxy. This rules out an interpretation of the "U" in terms of superposition of velocity distributions with differing mean velocities. In the regions between the two galaxies the dispersion profiles are often noisy and the reality of the dispersion increase is often less clear.

A significant difference between the new and the old data is the detection in the new data of local velocity dispersion maxima near the centers of the galaxies which show dispersion profiles rising outward. Examples are NGC 2673, 5718, 7236, 7237, and IC 1042. This structure is expected both when the U-shaped dispersion profiles are due to tidal heating and when they are due to light superposition, as both processes get inhibited near the center where the luminosity density and mass density of the galaxy are high. For our sample, the radius of the unperturbed region varies between 3″ and 5″ (i.e., 1.4 and 3.4 kpc).

6. SUMMARY

1. We have presented detailed kinematic measurements for several pairs of interacting elliptical galaxies and have used the resulting velocity profiles to elucidate various aspects of tidally induced dynamical and morphological evolution of galaxies.

2. We have confirmed the existence of U-shaped rotation and dispersion profiles in interacting ellipticals, which we previously reported (Borne & Hoessel 1985, 1988). U-shaped rotation and dispersion profiles are found in one-third and two-thirds of the galaxies, respectively. These U-shapes and the different variations seen (e.g., in NGC 751) substantiate our physical interpretation of these peculiar curves (Paper III): there is a tidal coupling between the orbit of the companion and the resonant prograde rotating stars in the kinematically disturbed galaxy. The U-shape is thus direct observational evidence for tidal coupling and hence a direct observational signature of tidal friction in action. That is, we are seeing the kinematic signatures of those stars that are responsible for the extraction of orbital energy and momentum from the binary

system, which will ultimately lead to the merger of the interacting galaxy pair (except in the most unbound encounters).

3. We have measured new features in the velocity profiles of interacting galaxies. For example: the S-shaped velocity curve in NGC 751, the occasional W-shaped dispersion profiles seen in some of the galaxies, and the general nonequilibrium velocity fields seen in most of the galaxies in the sample.

4. We have identified tidal kinematic and morphological evidence that supports the conjecture that elliptical galaxies often contain small embedded disk components.

5. We have used the new velocities to confirm the collision models that we published for K99, K175, and K564 (in Papers IV and VI). In nearly all instances, the new velocities, including those for previously unstudied position angles, substantiate the validity of those models. The few deviations from the models that we do see are generally well understood (e.g., a consequence of the manner in which we limited our parameter search for those models). As a result, the physical implications of those models (i.e., tidal coupling, tidal stripping, tidal heating, dynamical friction, and galaxy merging) are further substantiated by the data presented here. The new velocities for K46, K194, and Arp 171 (especially the unusual kinematics in K46) await a similar dynamical analysis, with a good chance of shedding further insight into the dynamics and evolution of interacting binary galaxies.

We wish to thank the Director of NOAO/KPNO for the generous allocations of telescope time that have been devoted to this project over the years. We also wish to thank Jeannette Barnes of NOAO for expert assistance in the initial stages of our data analysis and Jerry Kriss for help in the use of his FQUOT velocity analysis package. Several helpful suggestions by the referee are also gratefully acknowledged. This work was partially supported by a Scientific Collaboration Grant from NATO.

REFERENCES

Arp, H. C. 1966, ApJS, 14, 1
Balcells, M., Borne, K. D., & Hoessel, J. G. 1989, ApJ, 336, 655 (Paper VI)
Bender, R. 1988, A&A, 202, L5
Bender, R., Paquet, A., & Nieto, J.-L. 1991, A&A, 246, 349
Bertola, F., & Capaccioli, M. 1975, ApJ, 200, 439
Borne, K. D. 1984, ApJ, 287, 503 (Paper I)
———. 1988a, ApJ, 330, 38 (Paper II)
———. 1988b, ApJ, 330, 61 (Paper IV)
———. 1990a, in Dynamics and Interactions of Galaxies, ed. R. Wielen (Berlin: Springer), 196
———. 1990b, in IAU Colloq. 124, Paired and Interacting Galaxies, ed. J. W. Sulentic, W. C. Keel, & C. M. Telesco (Washington: NASA), 537
Borne, K. D., Balcells, M., & Hoessel, J. G. 1988, ApJ, 333, 567 (Paper V)
Borne, K. D., & Hoessel, J. G. 1985, BAAS, 17, 601
———. 1988, ApJ, 330, 51 (Paper III)
Borne, K. D., & Richstone, D. O. 1991, ApJ, 369, 111
Davies, R. L. 1981, MNRAS, 194, 879
Davies, R. L., Burstein, D., Dressler, A., Faber, S. M., Lynden-Bell, D., Terlevich, R. J., & Wegner, G. 1987, ApJS, 64, 581
Davies, R. L., Efstathiou, G., Fall, S. M., Illingworth, G., & Schechter, P. L. 1983, ApJ, 266, 41
de Vaucouleurs, G., de Vaucouleurs, A., Corwin, H. G., Jr., Buta, R. J., Paturel, G., & Fouqué, P. 1991, Third Reference Catalogue of Bright Galaxies (New York: Springer) (RC3)
Franx, M., & Illingworth, G. D. 1988, ApJ, 327, L55
Illingworth, G. D. 1977, ApJ, 218, L43
Jedrzejewski, R., & Schechter, P. L. 1988, ApJ, 330, L87
Karachentsev, I. D. 1972, Comm. Spec. Ap. Obs. USSR, 7, 3
———. 1980, ApJS, 44, 137
Madejsky, R. 1991, A&A, 247, 348
Madejsky, R., Bender, R., & Möllenhoff, C. 1991, A&A, 242, 58
Malumuth, E. M., & Kirshner, R. P. 1985, ApJ, 291, 8
McGlynn, T. A., & Borne, K. D. 1991, ApJ, 372, 31
Morgan, W. W., Kayser, S., & White, R. A. 1975, ApJ, 199, 545
Nieto, J.-L., Bender, R., Davoust, E., & Prugniel, P. 1990, A&A, 230, L17
Prugniel, P., Nieto, J.-L., & Simien, F. 1987, A&A, 173, 49
Rix, H.-W., & White, S. D. M. 1989, MNRAS, 240, 941
———. 1990, ApJ, 362, 52
Sargent, W. L. W., Young, P. J., Boksenberg, A., Shortridge, K., Lynds, C. R., & Hartwick, F. D. A. 1978, ApJ, 221, 731
Schechter, P. L. 1980, AJ, 85, 801
Tifft, W. G. 1982, ApJS, 50, 319
Tonry, J. L., & Davis, M. 1981, ApJ, 246, 666
White, S. D. M., Huchra, J., Latham, D., & Davis, M. 1983, MNRAS, 203, 701
Whitmore, B. C., McElroy, D. B., & Tonry, J. L. 1985, ApJS, 59, 1
Wirth, A., Smarr, L., & Gallagher, J. S. 1982, AJ, 87, 602